Proceedings of ASME-JSME-KSME Joint Fluids Engineering Conference 2011
AJK2011-FED
July 24-29, 2011, Hamamatsu, Shizuoka, JAPAN

AJK2011-LL003

A HIGH PERFORMANCE, LOW BACK PRESSURE JET EJECTOR

John F. Foss
Mechanical Engineering Department
Michigan State University
East Lansing, MI, USA

Alan R. Lawrenz
Mechanical Engineering Department
Michigan State University
East Lansing, MI, USA

ABSTRACT

Engine exhaust is used on a Cat wheel loader to induce ambient air through the engine compartment for thermal protection. Increased ambient (or secondary) flow ($\dot{m}_s$) was desired with a minimal impact on the muffler (i.e., plenum) pressure for the primary flow ($\dot{m}_p$). Jet tabs and a conical diffuser were combined to form a synergistic (highly non-linear) solution to this fluids engineering problem. The successful development strategy is clarified and the quantitative results for the entrainment rates ($\dot{m}_s$ as large as 180% of $\dot{m}_p$) are presented.

INTRODUCTION

High power-level equipment, such as the Caterpillar, Inc. wheel loaders (see Fig. 1), involve relatively high engine and exhaust system temperatures.

FIGURE 1. THE WHEEL LOADER ENGINE COMPARTMENT WITH CONE AND CYLINDRICAL EXHAUST STACK

The add-on equipment to meet the EPA Tier 4 emissions compliance adds to this intrinsic heat-load problem. The wheel loaders, like other high-power machines, are also subject to noise regulations. These acoustic emission requirements were met by reducing the openings in the engine enclosures (hoods). In combination, substantial increases in the underhood temperatures were experienced with the attendant concern for the integrity of the underhood components. The authors were given the challenge to increase the effectiveness of the system that induced a flow from the surroundings, through the underhood compartment and discharged it – along with the inducing engine exhaust – to the surroundings. This fluids engineering system is termed an "extractor."

Fig. 2, which has been prepared to show the geometric attributes of the MSU solution to the challenge, can also be used to clarify the original geometry as well as to clarify the components that were to be retained in the recommended flow system. The muffler (its upper portion that was used in the experiment) is shown in Fig. 2, the 110mm diameter muffler pipe and the conical contraction (cone) affixed to the top of the hood were to be unchanged. As shown in Fig. 1, the original flow system utilized a constant diameter exhaust pipe attached to the conical contraction. This exhaust pipe was terminated by an angled "rain hat." An additional constraint on the development of an improved extractor system, in addition to the geometric elements that were to be unchanged, was to impose a minimal increase in the flow system's back pressure. That is, a limited increase in the muffler pressure with respect to the atmospheric value was to be a part of the solution.

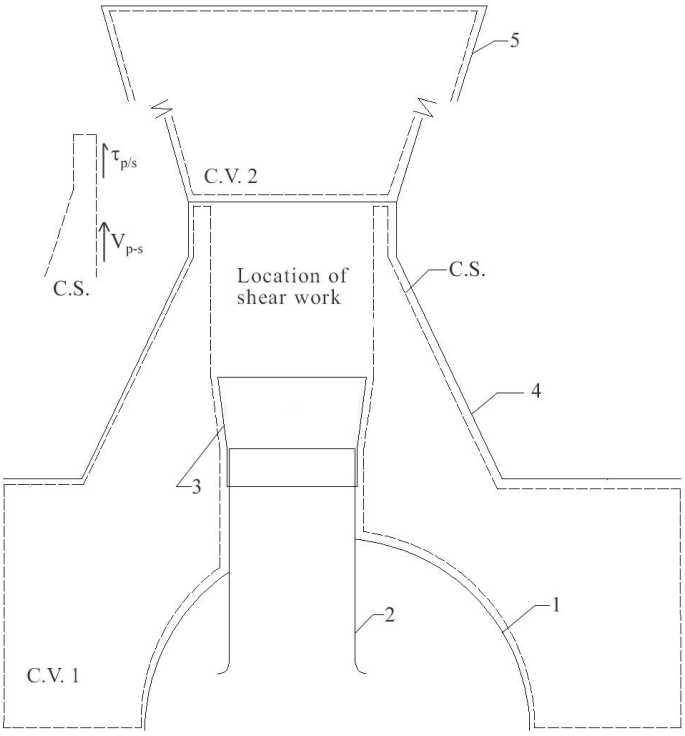

Legend

1. Muffler obtained from Cat
2. Muffler pipie: ID=110 mm, rounded inlet added (inlet added at MSU, not present on original equipment)
3. Transition piece, tabs not shown
4. Cone attached to top of the hood, original equipment
5. Diffuser added to cylindrical termination

FIGURE 2. SCHEMATIC REPRESENTATION OF THE PRIMARY AND SECONDARY FLOW PATHS

NOMENCLATURE

b tab dimension at its base where it attaches to the approach surface

$\dot{m}_p, \dot{m}_s, \dot{m}_T$ mass flow rates: primary, secondary and total (Eq. 5)

p pressure –sub p for primary plenum; –sub s for secondary plenum

p* reference to ambient pressure and made non-dimensional with ρV_p^2

$p^*_s]_L$ see Eq. 6

u,v,w instantaneous components of the velocity vector (Bohl and Foss (1999)

x streamwise distance from a designated origin

y,z spanwise, bi-normal coordinates in the Bohl and Foss (1999) study

A area

C_D discharge coefficient

D diameter of the muffler pipe

D_{in} exit diameter of the exhaust system cone

L length of the diffuser cones

L_{TP} length of the transition piece (TP)

N,S singular point designations: node, saddle, designated by their index values (Foss (2004)

T temperature

V velocity magnitude (Eq. 1)

V_p average velocity magnitude in the muffler tube

$\vec{V}_{p-s}$ velocity vector at the primary-secondary boundary downwind from the tabs (Eq. 1)

Greek Symbols

2ϕ included angle of the diffuser cone

ρ density

τ_{p-s} shear stress of primary fluid acting on the secondary fluid

JET TABS AS A CRITICAL ELEMENT OF THE EVOLVED SOLUTION

Enhanced mixing, with the attendant transfer of momentum between a high speed jet and its surrounding fluid, can be created by the use of "tabs." The effect of tabs on a jet flow was first studied by Bradbury and Khadem (1975). Further studies: Zaman, et al. (1991), Samimy, et al. (1993), Zaman, et al. (1994), Reeder and Samimy (1996), Foss and Zaman (1999), clarified the contributions of such tabs. Bohl and Foss (1999) introduced secondary tabs which further enhanced the mixing (and hence the entrainment effect) of tabs. Fig. 3, taken from the MS thesis of Bohl (1996), represents this enhanced mixing effect as shown by the isotachs (contours of constant streamwise velocity magnitudes) of a tabbed and a non-tabbed jet. Zaman, et al. (2011) provide a comprehensive review of tabbed jet flows.

The basic physics of the primary tab flow is to create a "pressure hill" on the bounding surface of the primary conduit. Since vorticity is introduced into a flow at a physical surface in the presence of a surface pressure gradient (as if the entering vorticity is "rolling down the hill"), there are streamwise vortex motions at the exit plane that propel the primary flow into the ambient region. The side view (Fig. 3b) shows the physical configuration of the primary tab (as studied previously) and the secondary tab (as introduced by Bohl and Foss (1999)). This added tab provides an attachment surface that helps the vortex motions advance into the ambient region for increased entrainment. The effects of these vortex motions are clearly revealed by the isotachs of Fig. 3. (See Bohl and Foss (1999) for a more complete description of the x>0 flow field).

Further insight into the tabbed jet flow field is provided by the X-array (hot-wire) data in two y-z planes as obtained by Bohl (1996) in his MS thesis; see Fig. 4 for the data at x/b=1.2 where b is the length of the tab's base. (These data also appear in Bohl and Foss (1999)). The calibrated X-array was used to record (u,v) and then (u,w) at discrete locations in these planes. The time-averaged $(\overline{v}, \overline{w})$ values were then used to plot the in-plane (x/b=1.2) streamlines as shown in Fig. 4. The streamlines show the two spiral nodes (vortex motions) that were introduced by the exit plane tabs.

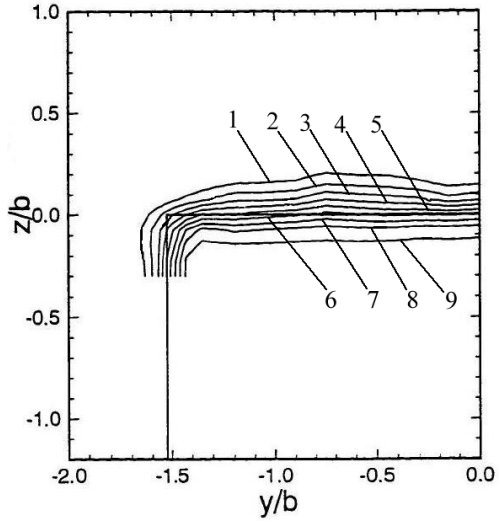

FIGURE 3A. NO INSTALLED TABS

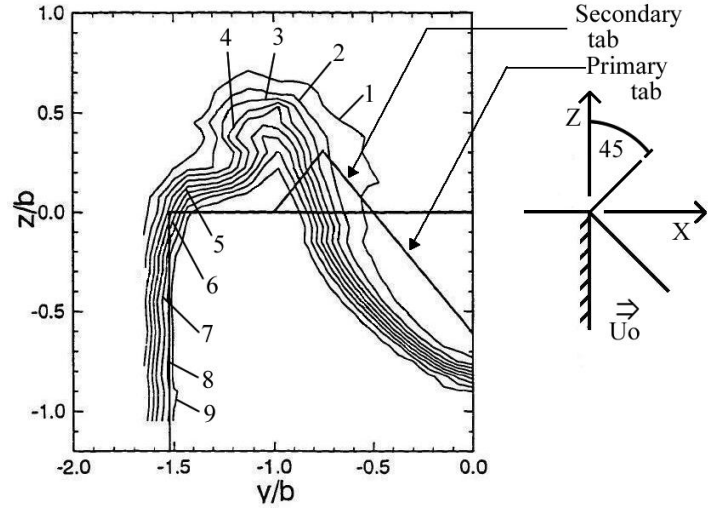

FIGURE 3B. PRIMARY AND SECONDARY TABS INSTALLED

FIGURE 3. ISOTACHS: CONTOURS OF CONSTANT STREAMWISE VELOCITY (ū); x/b=1.2

1	2	3	4	5	6	7	8	9
0.15	0.25	0.35	0.45	0.55	0.65	0.75	0.85	0.95

Given the opportunities for errors in the inferred streamlines, it was beneficial to evaluate the integrity of the images using the topological considerations presented in Foss (2004) and Foss (2007). Specifically, the streamlines identify a collapsed sphere whose perimeter (solid curves) is interrupted by two holes (dashed curves). The latter are openings at which the vector directions are uniformly inward or outward. The inferred streamline pattern – with its two saddles and two nodes (vortex motions) – is in agreement with the topological constraint. The Euler characteristic (X) is zero given: $X = 2 - \Sigma holes - 2\Sigma handles = \Sigma N - \Sigma S$.

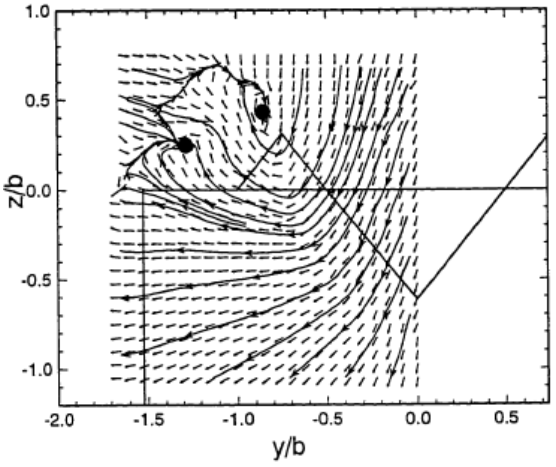

FIGURE 4A. STREAMLINES FROM $\bar{v}, \bar{u}$ MEASUREMENTS (MAGNITUDES ARE NOT SHOWN)

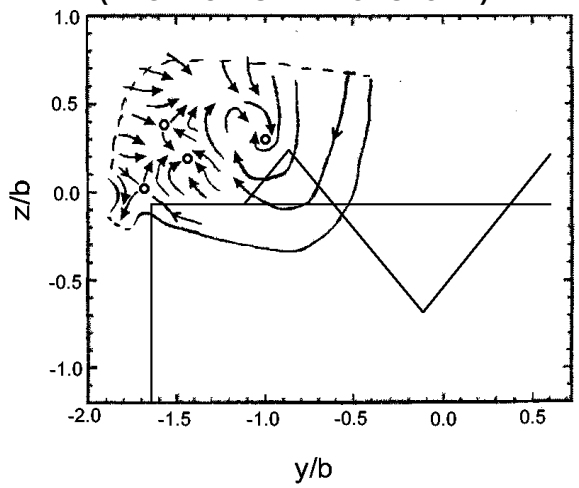

FIGURE 4B. CLARIFICATION OF THE IN-PLANE VECTOR VIELD

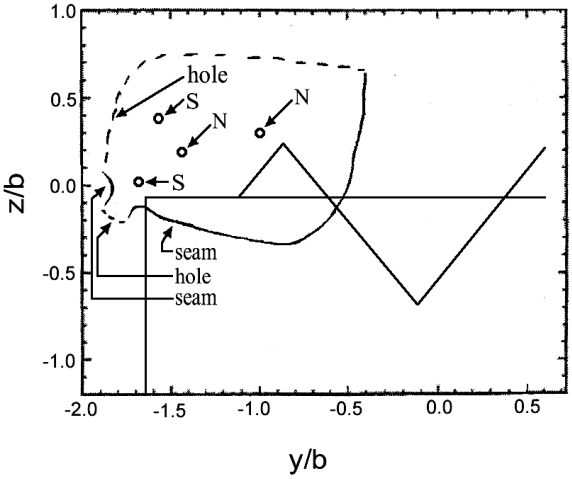

FIGURE 4C. COLLAPSED SPHERE REPRESENTATION WITH ----- AS THE PERMITTER SEAM AND ----- DESIGNATING A HOLE

FIGURE 4. VECTOR FIELD INFORMATION RECOVERED FROM THE COMBINED X-ARRAY MEASUREMENTS; x/b=1.2

GEOMETRIC MODIFICATIONS TO ACHIEVE AN ENHANCED EXTRACTOR PERFORMANCE

Tabs

The standard exhaust system geometry made use of a 110mm diameter circular pipe from the muffler interior to a location below the throat of the cone that was attached to the top of the hood. This geometry was modified in the present study by adding a transition piece (round-to-polygon) that was terminated by the addition of primary and secondary tabs. Three transition pieces were developed; see Fig. 5. As shown, these pieces vary in the relative size of the primary tab (base=b) and that of the secondary tab (base=nb). The muffler pipe diameter (D=110mm) was constant for all transition pieces as were their streamwise lengths (L_{TP}) where $L_{TP}/D=0.691$. Since the tabs' effectiveness depends upon relatively high speed fluid near the surface, it was also necessary to install a rounded inlet on the muffler tube. (The standard geometry involved a reentrant-entrance).

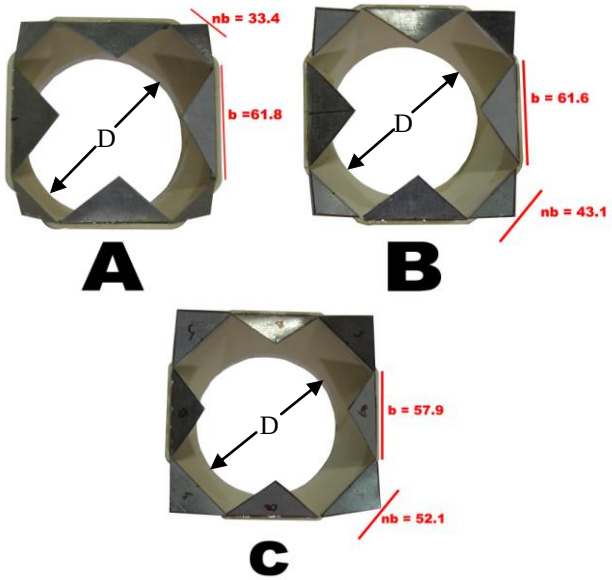

Figure 5a Plan view

Note: D = 110mm

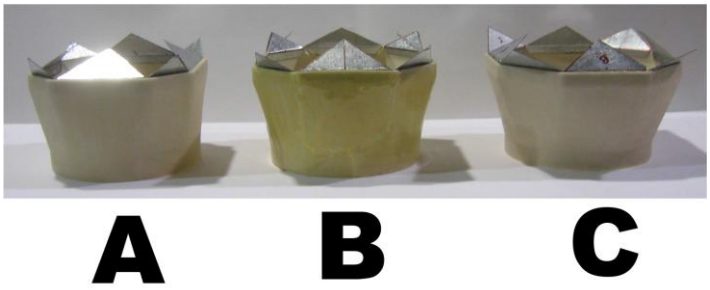

Figure 5b. Perspective view

FIGURE 5. DESCRIPTION OF THE THREE TRANSITION PIECES

Diffuser

A second significant modification (as shown in Fig. 2) to the standard geometry was to replace the cylindrical exhaust pipe with a conical diffuser. The four diffuser cones are represented in Table 1 and shown (via a photograph) in Fig. 6. The common throat diameter (D_{in}) was established by the existing conical contraction of the standard geometry and each diffuser length was 55cm or $L/D_{in}=3.14$.

FIGURE 6. PHOTOGRAPH OF THE FOUR DIFFUSERS USED IN THIS STUDY

TABLE 1: DIFFUSER SPECIFICATIONS
Diameters (m)

Diffuser	Throat ($D_{t,m}$)	Exit ($D_{e,m}$)	2ϕ
1	0.173	0.234	6.41
2	0.173	0.259	9.01
3	0.173	0.280	11.2
4	0.173	0.302	13.5

ANALYTICAL CONSIDERATIONS

From the perspective of the induced or secondary flow from the ambient, the engine exhaust – or the primary flow – serves as the "prime mover." Specifically, the motive effect is the work rate of the primary flow acting on the secondary flow. Hence, it is appropriate to describe the extractor using the First Law of Thermodynamics in control volume form; see, for example, Munson, et al. (2002) and Potter and Foss (1975). Fig. 2 provides two control volumes for this purpose.

Notwithstanding the complex three-dimensional flow field within CV1, one can appreciate that a time-mean stream surface separates the primary from the secondary flow. The motive effect for the latter derives from the shear stresses of the primary flow acting on the secondary fluid ($\vec{\tau}_{p/s}$) with a corresponding velocity ($\vec{V}_{p-s}$) at the same location. The spatial integral of this scalar-product within CV1 is the work rate term (LHS) of the First Law of Thermodynamics; see (1).

$$\int \vec{\tau}_{p/s} \cdot \vec{V}_{p-s} dA_{p-s} = \int_{cs} \rho \left[\frac{V^2}{2} + p/\rho \right] \vec{V} \cdot \hat{n} dA + \sum k \frac{V^2}{2} \qquad (1)$$

where the left-hand side is the work rate of the primary fluid (p) on the secondary fluid (s). (By convention, the work rate term in (1) should be represented with a negative sign since the thermodynamic system – the secondary fluid – is to do work on the surroundings. Using the complementary work rate: "primary-on-secondary," absorbs that negative sign as shown in (1)). Equation 1, written in terms of instantaneous quantities, "hides" considerable complexity albeit it is accurate as stated. If the conventional "mean plus fluctuation" description for each variable were introduced, those substitutions would lead to substantially more terms given the correlations that exist for the fluctuating terms. For the present purpose, it is sufficient to utilize (1) to qualitatively describe the operative physical effects. Specifically, the scalar product of the two left-hand-side vectors is greater than zero. The right-hand side shows the net kinetic energy flux (a positive term for CV1) and the net flow work (a negative term) given the pressure drop from the secondary plenum (or underhood region) to the throat (t) at the exit of CV1. The term: $\sum kV^2/2$, represents the dissipative losses, a positive term albeit with a "negative effect."

The second control volume is used to describe the beneficial effects of the diffuser. Two factors are important in this regard: i) the outward directed flow from the tabs (see the isotach pattern of Fig. 3b) plays a strong role in energizing the diffuser wall region which allows for a relatively large pressure increase for this control volume, and ii) the strong pressure rise for control volume 2 with its exit condition at atmospheric pressure implies a "sink effect" for the secondary flow between the underhood region and the throat of the cone. The pressure rise (for control volume 2) also reduces the required muffler pressure level to deliver a given primary flow rate.

The essential message is that the tabs and the diffuser form a mutually beneficial synergistic effect that significantly enhances the individual contribution of either element. This was also demonstrated by using the tabs with the cylindrical stack and the diffuser without the tabs. Very little gain was obtained (over that of the standard geometry) with both of these configurations.

THE EXPERIMENTAL FLOW SYSTEM

A flow system, that allowed one centrifugal blower to provide $\dot{m}_p$ and $\dot{m}_s$, was constructed for the subject investigation; see Fig. 7. Fig. 7a is a plan view of the flow system that reveals most of its elements. Fig. 7b clarifies the flow path from the 1.865m long inlet plenum (that is fed by the two metering nozzles) to the 37V Buffalo Forge blower whose pressurized output is turned into the upward direction (past the "flow control throttle") and into the plenum that feeds both the primary and the secondary flow paths. (The flow control throttle: FCT, is located in this vertical flow path). The "secondary control throttle" is located at the dashed line (identified as "A") of Fig. 7a. Note that the transition piece (with its tabs) and the conical diffuser are not shown in Fig. 7.

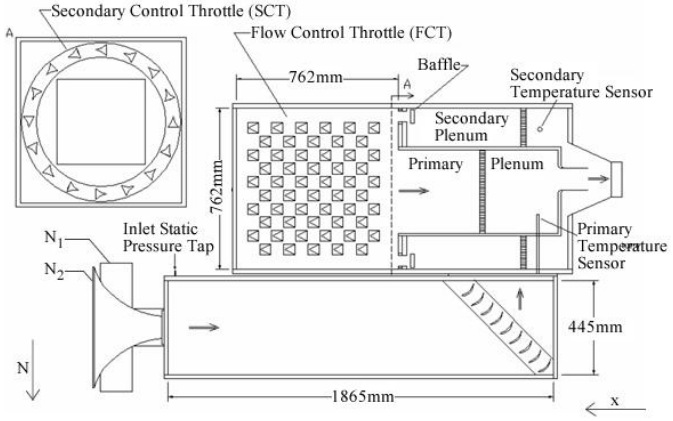

FIGURE 7A. PLAN VIEW OF THE EXPERIMENTAL FLOW SYSTEM
Note N1, N2 are vertically displaced metering nozzles

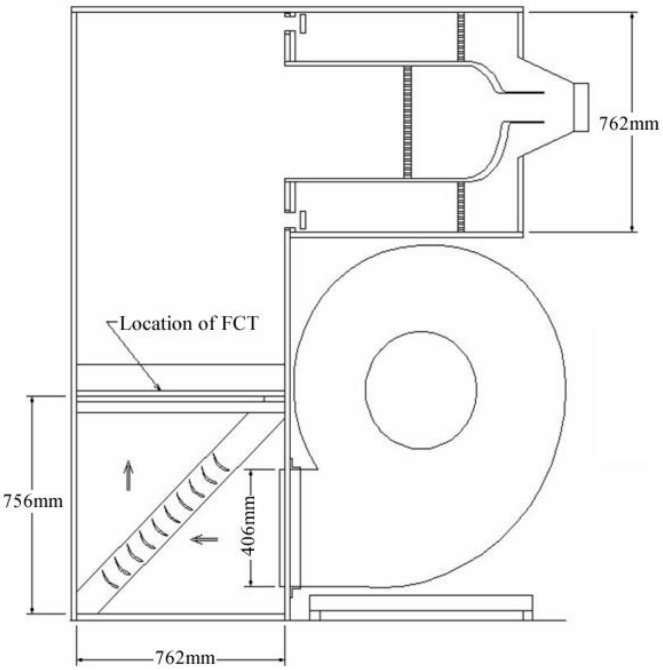

FIGURE 7B. FLOW SYSTEM ELEVATION VIEW FACING SOUTH

FIGURE 7. SCHEMATIC REPRESENTATION OF THE EXPERIMENTAL FLOW SYSTEM

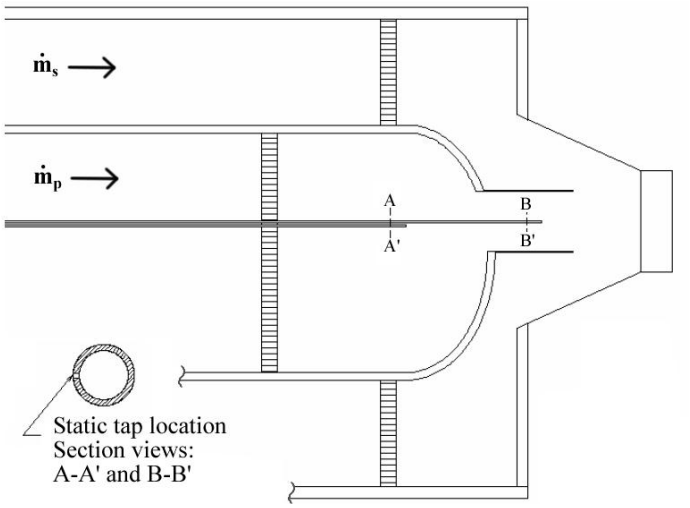

FIGURE 8A. ELEVATION VIEW

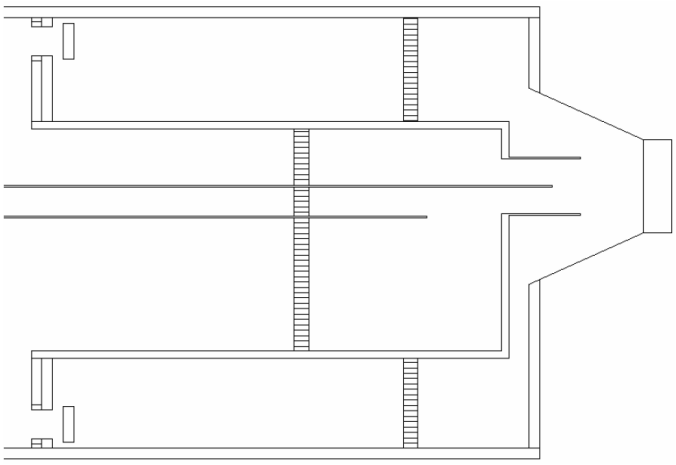

FIGURE 8B. PLAN VIEW

FIGURE 8. FLOW PATHS FOR THE PRIMARY AND SECONDARY FLOWS AND THE PRESSURE PROBES FOR THE $\dot{m}_p$ MEASUREMENT

Fig. 8 presents the (unconventional – but effective) strategy to determine the primary mass flow rate. Specifically, the cylindrical tubes that extended to the primary plenum and to the muffler pipe were capped at their farthest extent and a side-wall tap allowed the local static pressure to be recorded. The flow measurement strategy is described below.

Fig. 9 completes the flow system by showing the conical diffuser added to the cone.

FIGURE 9. ELEVATION VIEW WITH DIFFUSER CONE ATTACHED TO CAT CONE

FLOW MEASUREMENT STRATEGY

The flow measurement objective was to determine the magnitude of the secondary flow rate: $\dot{m}_s$, with respect to the magnitude of the primary flow rate: $\dot{m}_p$, as the geometric parameters of the flow system were varied. Since direct viscous effects could reliably be understood to play a minor role, the actual Reynolds numbers were of secondary importance in the identification of the $\dot{m}$ ratios: $\dot{m}_s / \dot{m}_p$. Nominal values for the inlet nozzle discharge coefficients were available and, with this measurement strategy, acceptable.

The following details describe the measurement strategy to obtain $\dot{m}_p$ when $\dot{m}_s = 0$. See Fig. 8 for the pressure values that were calibrated to identify the $\dot{m}_p$ value. Specifically, these two probes were used to record the static pressures within the primary plenum (i.e., the partial muffler) and the muffler pipe upwind from the transition piece. It was possible to secure the secondary flow throttle valve such that a condition of $\dot{m}_s = 0$ was satisfactorily obtained. With this condition, the flow control throttle was used to vary the $\dot{m}_p$ value while $(p_{atm} - p_{inlet})$ was recorded such that

$$\dot{m}_p = \sum_{k=1}^{2} [c_D]_k \rho A_k V_{inlet} \qquad (2)$$

where k=1,2, designate the two nozzles that deliver flows to the inlet plenum. The inlet velocity is given by

$$V_{inlet} = [2(p_{atm} - p_{inlet})/\rho]^{1/2}. \qquad (3)$$

With this condition $(\dot{m}_s = 0)$ and a known $\dot{m}_p$ value, the primary flow metering technique:

$$\dot{m}_p = f(\Delta p) \qquad (4a)$$

could be established as

$$\dot{m}_p = K(\Delta p)\rho A_{pipe}\sqrt{2\Delta p/\rho} \qquad (4b)$$

where Δp is the pressure difference recorded by the side-wall pressure taps of the two cylindrical probes shown in Fig. 8.

Flow system dissipative effects provide elevated temperature (T) effects such that $T_{primary}>T_{amb}$ and this is accounted for in the evaluation of ρ for (4). Beyond that adjustment, Equation 4 can be understood to define K(Δp) since all other terms are directly measured.

Given that $\dot{m}_p$ and the total flow rate: ($\dot{m}_T$) could be directly measured when the secondary flow path was opened, $\dot{m}_s$ was inferred from the mass-flow balance as

$$\dot{m}_s = \dot{m}_T - \dot{m}_p \qquad (5)$$

The high Reynolds number of the primary flow path and the large area ratio from its plenum to the muffler pipe is considered to provide a reliable $\dot{m}_p$ value when $\dot{m}_s>0$. The ratio: $\dot{m}_s/\dot{m}_p$ is the principal dependent variable of this study.

RESULTS AND DISCUSSION

Basic Considerations

Sixteen geometric conditions were evaluated: TPA, TPB, TPC and No TP were paired with each of the four diffusers (1…4). (It is important to note that the No TP case did involve a constant diameter extension of the muffler pipe to the same level as that for the base of the taps) Starting with the Secondary Control Throttle (SCT) in the wide open position, which gave the maximum flow rate for the given geometry, and then closing the SCT allowed $(\dot{m}_s/\dot{m}_p)$ to be determined as a function of $p_s^* = ([(p_s - p_{atm})/\rho V_p^2])$. Note that the condition $p_s^*<0$ for the prototype application represents the pressure drop to move the outside air into the underhood compartment. Fig. 10 presents a representative result for the mass flow rate ratio as a function of p_s^*. The linear region: $p_s^*]_L \le p_s^* \le 0$, can be represented by the polynomial form:

$$\dot{m}_s/\dot{m}_p = a + b\frac{p_s^*}{|p_s^*]_L|} \qquad (6)$$

The non-dimensional plenum pressure: p_p^*, which is defined as $p_p^*=(p_\rho - p_{atm})/\rho V_p^2$, can also be obtained for the 16 conditions. Table 2 provides a complete representation of these basic data.

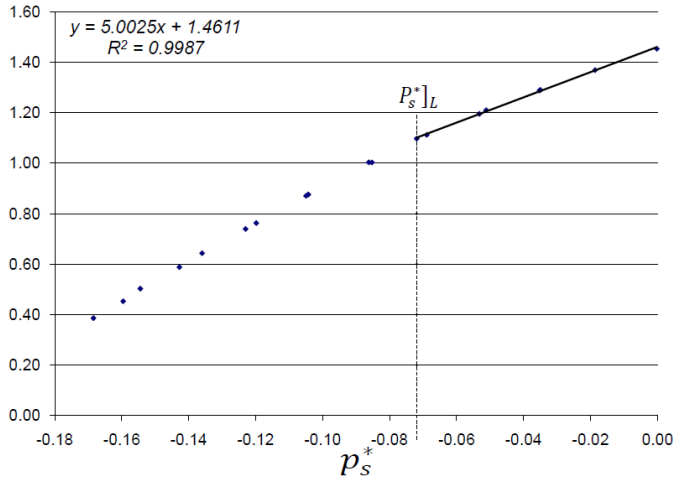

FIGURE 10. A REPRESENTATIVE PLOT OF $\frac{\dot{m}_s}{\dot{m}_p} = f(p^*_s)$ FOR TP B AND DIFFUSER 2

TABLE 2 $\dot{m}_s/\dot{m}_p$ DEPENDENCIES UPON P_S^* AND P_P^* FOR THE GEOMETRIC PARAMETERS

Transition Piece	Diffuser	$\left.\frac{\dot{m}_S}{\dot{m}_P}\right]_{p_S^*=0}$	$\frac{d}{dp_S^*}\left(\frac{\dot{m}_S}{\dot{m}_P}\right)$	$p_s^*]_L$	p_P^*
TP A	1	1.50	4.67	-0.163	0.867
	2	1.73	5.66	-0.169	0.835
	3	1.82	5.89	-0.074	0.82
	4	1.81	5.44	-0.172	0.813
TP B	1	1.29	4.67	-0.091	0.699
	2	1.46	5	-0.072	0.68
	3	1.51	5.46	-0.082	0.656
	4	1.53	5.73	-0.068	0.657
TP C	1	1.2	4.22	-0.117	0.598
	2	1.27	5	-0.115	0.588
	3	1.32	5.2	-0.126	0.602
	4	1.23	4.26	-0.045	0.62
No TP	1	0.964	5.02	-0.072	0.703
	2	0.924	5.88	-0.038	0.696
	3	0.798	5.08	-0.07	0.714
	4	0.701	5.27	-0.054	0.722

Diagnostic Considerations to Clarify the Flow-Physics of this Extractor

A subset of the complete body of data: $\dot{m}_s / \dot{m}_p = f(p_p^*)$ for $p_s^*=0$, is presented in Fig. 11. The following items are considered to be quite instructive regarding the flow-physics of this extractor flow.

1) The two larger angle diffusers: 3,4, combined with the two larger primary tab assemblies: A,B, show self-consistent behavior. Specifically, $\dot{m}_s / \dot{m}_p$ increases and p_p^* decreases as the diffuser angle (2ϕ) is increased from 6.41 to 11.2 degrees. (The further increase of 2ϕ to 13.5 degrees for TPA did not have a distinctive influence on the $\dot{m}_s / \dot{m}_p = f(p_p^*)$ relationship albeit a further gain in the ratio was observed for TPB).

2) In contrast, TPC gains maximum performance with diffuser 3 and the dependence of $\dot{m}_s / \dot{m}_p$ on p^*_p and 2ϕ is weak.

3) The "No TP" case shows the opposite relationship of $\dot{m}_s / \dot{m}_p$ =f(2ϕ) and g(p_p^*) compared with the data for TPA and TPB. This observation clearly indicates that a strong coupling exists between the diffuser and the tabs.

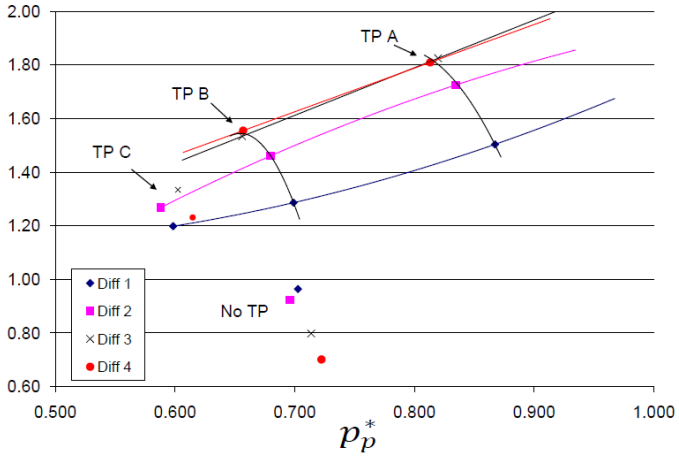

FIGURE 11. COMPREHENSIVE REPRESENTATION OF THE $\frac{\dot{m}_s}{\dot{m}_p} = f(\ p^*_p, p^*_s = 0)$ RESULTS FOR FOUR DIFFUSERS, THREE TPs AND A CYLINDRICAL TERMINATION (NO TP)

4) A second indication of the clear relationship between the diffuser cone and the tabs is present in the p_p^* values for TPC and the No TP condition. Considering the clustered averages of the p_p^* values for these two cases, it is apparent that p_p^* is reduced and $\dot{m}_s / \dot{m}_p$ is increased by the addition of the tabs even though TPC was a relatively "poor performer" compared with TPB and TPA.

Fig. 12 has been prepared to show the influence of the diffuser angle (2ϕ) on the p_p^* and the ($\dot{m}_s / \dot{m}_p$) values. The trends are most clearly shown for the "higher performing" TPA and TPB configurations. That is, the secondary flow was increased for the larger 2ϕ values and the tabs-plus-diffuser combination lowered the required plenum pressure (p_p^*) as 2ϕ was increased. In contrast, TPC and the No TP conditions did not exhibit these favorable trends albeit for obviously different reasons. TPC, unlike TPA and TPB, introduced too large of an area expansion from the fixed D value of the inlet pipe. Conversely, since p_p^* did not respond to changes in 2ϕ for the No TP case, it can be understood that the primary flow did not experience a "diffuser effect" given the large area ratio of the diffuser cones with respect to the muffler pipe. However, the increased $\dot{m}_s / \dot{m}_p$ values as 2ϕ decreased to its minimum value for the No TP case indicates that the secondary flow gained an advantage from the "diffuser effect" when the primary flow was delivered to the same streamwise location via a constant diameter pipe.

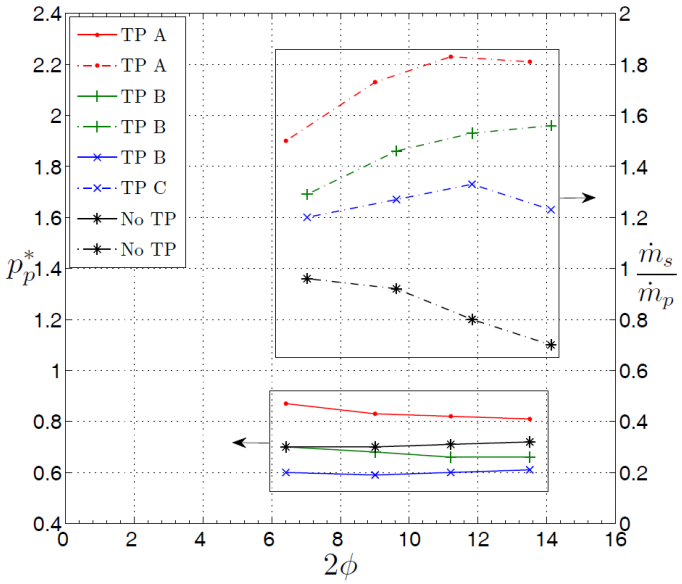

FIGURE 12. THE PLENUM PRESSURE (p^*_p FOR p^*_s=0) AND THE MASS FLOW RATIO ($\dot{m}_s/\dot{m}_p$) AS A FUNCTION OF THE DIFFUSER INCLUDED ANGLE (2ϕ)

SUMMARY

A combination of fluids engineering basic elements: i) a rounded entrance for the muffler pipe, ii) primary and secondary tabs, and iii) a conical diffuser were combined to substantially enhance the performance of an extractor. Quantitative values for the magnitude of the secondary (entrained) flow with respect to the primary flow have been obtained and presented in a manner that will allow interpolation between the discrete states. Similarly, the (modest) back pressure (p_p^*) penalty for the highest performing configuration (diffuser 3 with TPA) has been identified. Significantly, there is essentially no p_p^* penalty for the second highest performing condition: TPB with diffusers 3 and 4.

REFERENCES

[1] Bohl, D.G., 1996. "An Experimental Study of the Near Field Region of a Free Jet with Passive Mixing Tabs," MS Thesis, Michigan State University.

[2] Bohl, D.G. and Foss, J.F., 1999. "Near Exit Plane Effects Caused by Primary and Primary-Plus-Secondary Tabs," *AIAA Journal*, 37(2), pp. 192-201.

[3] Bradbury, L.J.S., and Khadem, A.H., 1975. "The Distortion of a Jet by Tabs," *Journal of Fluid Mechanics*, **70**.

[4] Foss, J.F., 2004. "Surface Selections and Topological Constraint Evaluations for Flow Field Analyses," *Experiments in Fluids*, Springer-Verlag, **37**, pp. 883-898.

[5] Foss, J.F., 2007. *Springer Handbook of Experimental Fluid Mechanics*, Chapter 13, Springer-Verlag, Berlin.

[6] Foss, J.K. and Zaman, K.B.M.Q., 1999. "Large- and small-scale vortical motions in a shear layer perturbed by tabs," *J. Fluid Mech.*, **382**, 307-329.

[7] Munson, B.R., Young, D.F. and Okiishi, T.H., 2002. *Fundamentals of Fluid Mechanics*, John Wiley & Sons.

[8] Potter, M.C., and Foss, J.F., 1975. *Fluid Mechanics*, The Ronald Press Co., New York. (Now published by Great Lakes Press, Okemos, MI).

[9] Reeder, M.F. and Samimy, M., 1996 "The evolution of a jet with vortex-generating tabs: real-time visualization and quantitative measurements," *J. Fluid Mech.*, **311**, pp. 73-118.

[10] Samimy, M., Zaman, K.B.M.Q. and Reeder, M.F., 1993. "Effect of tabs on the flow and noise field of an axisymmetric jet," *AIAA Jour.*, **4**, 1251-1258.

[11] Zaman, K.B.M.Q., Samimy, M. and Reeder, M.F., 1991. "Effect of Tabs on the Evolution of an Axisymmetric Jet," Eighth Symposium on Turbulent Shear Flows, Paper 25-5.

[12] Zaman, K.B.M.Q., Reeder, M.F., and Samimy, M, 1994. "Control of an axisymmetric jet using vortex generators," *Physics of Fluids A*, **6**(2), pp. 778-793.

[13] Zaman, K.B.M.Q., Bridges, J.E., and Huff, D.L., "Evolution from 'Tabs' to 'Chevron Technology' -- a Review," NASA Glenn Research Center Cleveland, OH, USA, to appear in the *International Journal of Aeroacoustics*.